J Stat Phys (2010) 139: 915–939
DOI 10.1007/s10955-010-9965-0

Moments for Tempered Fractional Advection-Diffusion Equations

Yong Zhang

Received: 10 October 2009 / Accepted: 5 April 2010 / Published online: 21 April 2010

Abstract This paper develops moment formulas for exponentially tempered, fractional advection-diffusion equations (TFADEs) that transition from anomalous to asymptotic diffusion limits over time. Exact analytical expressions or series representations for spatial moments up to the fourth order are derived by integral transform or asymptotic expansion approach. A fully Lagrangian solver, cross verified by an implicit Eulerian approach, is also developed to calculate numerically the complete evolution of moments for the TFADEs with complex initial and boundary conditions. Moment analysis identifies the diffusion equation that attracts the tempered anomalous diffusion in the long time limit. Fitting of moments measured at two end members of alluvial systems checks the applicability of moment analysis in understanding real diffusion.

Keywords Spatial moments · Tempered Lévy motion · Anomalous diffusion

1 Introduction

Fractional-derivative models have been increasing in popularity in the last decade for characterizing anomalous diffusion in almost all natural systems [44–46]. For example, in the hydrology science, the fractional-derivative models have been developed to describe anomalous diffusion for contaminant transport through heterogeneous porous or fractured media [11, 27, 31, 62]. In particular, the scaling limit of the continuous time random walk (CTRW) with a jump distribution function $\phi(x) \sim x^{-(1+\alpha)}$ $(1 < \alpha < 2)$ produces the superdiffusive transport model. The stable Lévy distribution for particle displacement contains arbitrarily large jumps and has divergent spatial moments higher than the first order. Fast transport events are well documented, but an unlimited power-law density (without any natural cutoff) and the resultant infinite moments may not be feasible for some physical processes [7, 38–40, 42, 43]. For example, for contaminant transport in natural geological formations, the arbitrarily large displacements for contaminants may not be feasible due to the typically

Y. Zhang (✉)
Desert Research Institute, Las Vegas, NV 89119, USA
e-mail: yong.zhang@dri.edu

finite water velocity, the possible decorrelation in particle trajectories along preferential flow paths [10], and/or the unavoidable scale of heterogeneity [58], which all can lead to a rectifiable sample path for solute particle during one single jump.

The truncated Lévy process is the logic extension of the standard Lévy process to capture the convergent spatial moments and the natural cutoff of power-law distributions present in real physical systems. The truncated stable Lévy flights proposed first by Mantegna and Stanley [38, 39] discard large jumps directly [37]. Exponentially tempered stable processes were then proposed by Koponen [33] and Boyarchenko and Levendorskiĭ ([5], Chap. 3) as a smoother alternative without a sharp cutoff. The resultant Lévy motion models, which are known as KoBoL processes (from *Koponen*, *Boyarchenko* and *Levendorskiĭ*) in the mathematical finance community [6, 9, 28, 41], cool arbitrarily large movements (such as the stock price movements) and therefore ensure finite moments (see page 71 in [5] and page 56 in [54]). Exponentially tempered Lévy motion models have drawn attention recently in the statistical physics as well as the applied mathematics community [2, 10, 52], probably due largely to the tractability of the tempered process. The tempered process remains an infinitely divisible Lévy process whose governing equation can be identified [54], and its transition densities can be computed at any scale [2].

This study continues previous efforts in moment analysis by developing moment formulas for novel tempered models. Systematical analysis of moment evolution helps to understand the nature of physical processes and identify the long time limit of the tempered anomalous diffusion. We then expand the application to ground water hydrology by simulating real-world evolution of moments measured in solute transport processes. Such detailed comparison with field measured moment data has been limited in literature.

The rest of the paper consists of five sections. The appropriate physical models are first built in Sect. 2, by extending the tempered fractional-order advection-diffusion equation (TFADE) proposed in above literature. In Sect. 3, the asymptotic expansion approach is applied to derive the series representations of moments up to the fourth order (including mass, mean, variance, skewness and kurtosis) for the extended TFADEs containing both space and time fractional derivatives. Numerical approaches are then developed in Sect. 4 to approximate the complete growth of spatial moments for the TFADEs. The extended TFADE models and the corresponding spatial moments are then checked against field observations in heterogeneous porous media in Sect. 5. Conclusion is drawn in Sect. 6.

2 The Tempered Fractional-Order Advection-Diffusion Equation Model

Various versions of fractional-derivative models have been developed to describe different physical processes. The physical model based on fractional dynamics and describing solute transport in natural systems can be built by following the space-time fractional-order partial differential equation (FPDE) proposed by Cartea and del-Castillo-Negrete [10]

$$ {}_0\mathcal{D}_t^{\gamma} P(x,t) = -[V + D\alpha\theta\lambda^{\alpha-1}]\partial_x P(x,t) - D\mathcal{D}_x^{\alpha,\lambda} P(x,t) - D\lambda^{\alpha} P(x,t), \qquad (1) $$

which is the scaling limit of the continuous time random walk with exponentially truncated Lévy jump distributions. Here the symbol ${}_0\mathcal{D}_t^{\gamma}$ denotes the γ-order ($0 < \gamma < 1$) Caputo fractional derivative in time t, V $[LT^{-1}]$ is the velocity, D $[L^{\alpha}T^{-1}]$ is the fractional dispersion coefficient, λ $[L^{-1}]$ is the truncation parameter, α [dimensionless] ($1 < \alpha < 2$ in this study) is the order of the stable density in space, $-1 \le \theta \le 1$ [dimensionless] is the skewness coefficient of the Lévy density, and $\mathcal{D}_x^{\alpha,\lambda}$ denotes the truncated fractional derivative operator.

$\mathcal{D}_x^{\alpha,\lambda}$ is defined as

$$\mathcal{D}_x^{\alpha,\lambda} = le^{-\lambda x}{}_{-\infty}\mathcal{D}_x^{\alpha} e^{\lambda x} + re^{\lambda x}{}_x\mathcal{D}_{\infty}^{\alpha} e^{-\lambda x}, \tag{2}$$

where $l = -\frac{(1+\theta)}{2}$ and $r = -\frac{(1-\theta)}{2}$. ${}_{-\infty}\mathcal{D}_x^{\alpha}$ and ${}_x\mathcal{D}_{\infty}^{\alpha}$ denote the Riemann-Liouville fractional derivatives:

$${}_{-\infty}\mathcal{D}_x^{\alpha} f = \frac{1}{\Gamma(2-\alpha)} \frac{\partial^2}{\partial x^2} \int_{-\infty}^{x} \frac{f(y)}{(x-y)^{\alpha-1}} dy, \tag{3a}$$

$${}_x\mathcal{D}_{\infty}^{\alpha} f = \frac{1}{\Gamma(2-\alpha)} \frac{\partial^2}{\partial x^2} \int_{x}^{\infty} \frac{f(y)}{(y-x)^{\alpha-1}} dy. \tag{3b}$$

The above fractional derivatives are space nonlocal operators of convolution type [47, 50]. The value of the left-handed fractional derivative (3a) at a local point x depends on the function values at all the points in the interval $(-\infty, x)$ (i.e., the space left of x), while the value of the right-handed fractional derivative (3b) at x depends on the function values in the interval (x, ∞) (the right domain). Also note that the left hand side term ${}_0\mathcal{D}_t^{\gamma}$ in (1) captures the subdiffusive effect. When subdiffusion does not exist, $\gamma = 1$ and the FPDE (1) reduces to the KoBoL model [9, 41]. The FPDE (1) is also a tempered, fractional-order advection-diffusion equation. To distinguish it from the other TFADEs developed below, we name (1) as the original TFADE. High order spatial moments such as skewness and kurtosis (which measure the deviation from Gaussian and identify the non-Gaussian shape of anomalous diffusion) for model (1) have not been derived before. This study provides first the exact formula and evolution behavior of all moments up to the fourth order for (1) (see Appendix A), which can be compared to the moments for the other TFADEs discussed below.

Two critical modifications of the original TFADE (1) are needed to capture real-world solute transport. Firstly, the maximally skewed Lévy density is needed (i.e., $\theta = 1$ in (2) to capture fast motions of solute particles in fractal media, similar to the FMLS (finite moment log stable) process [8]. The modification results in the following TFADE model:

$$\frac{\partial^{\gamma} C(x,t)}{\partial t^{\gamma}} = -V \frac{\partial C(x,t)}{\partial x} + D\left\{ e^{-\lambda x} \frac{\partial^{\alpha}[e^{\lambda x} C(x,t)]}{\partial x^{\alpha}} - \alpha\lambda^{\alpha-1} \frac{\partial C(x,t)}{\partial x} - \lambda^{\alpha} C(x,t) \right\}, \tag{4}$$

where C $[ML^{-3}]$ is the density or solute concentration in ground water hydrology. The Caputo fractional derivative for time is used in the following (unless specified), considering its convenience over the Riemann-Liouville derivative [22, 50]. Derivation of (4) with $\gamma = 1$ can be found in [2], where the tempered stable was defined simply as the multiplication of the Lévy measure and an exponential function $\exp(-\lambda x)$.

Model (4) contains a single-side (left-handed) space fractional derivative that simplifies the symmetric Riesz-Feller space-fractional derivative $\partial^{\alpha}/\partial|x|^{\alpha}$ (for example, see (2) in [34] and (55) in [53]) and the asymmetric two-side fractional derivative used in (1). The physical reason for choosing the maximum skewness coefficient ($\theta = 1$) has been discussed by various researchers in the hydrology community (see [26, 32, 55, 60], among many others). Here we introduce the discussion briefly, to provide background. The probability for a solute particle to jump forward is $(1+\theta)/2$, while the backward jump probability is $(1-\theta)/2$ [55]. The skewness coefficient θ is equal to 1 when solute disperses preferentially at velocities ahead of the mean velocity [55, 60]. Large tracer jumps only occur downward in natural media under ambient flow conditions. For example, natural rivers and streams may contain various forms of small-scale reverse flows (induced for example by bends and pools, side

pockets, zones between dikes, and/or turbulent eddies), but there is typically no large-scale backward dispersion for a solute particle to return to the upper boundary far away from its current location [62]. In other words, the concentration change at a local point should not depend on the net dispersive flux far away downstream, and hence the right-handed fractional derivative (3b) does not apply here. This was confirmed by the analysis of velocity distributions in [26, 32]. Strictly speaking, the contaminant transport through natural media tends to exhibit the maximum skewness due to the fast transport of solute through preferential flow paths at all scales [60]. The maximum skewness is also consistent to the space nonlocal dispersive flux used by the nonlocal dispersive constitutive theories proposed by the fluid mechanics community [16, 17]. In addition, when $\lambda \to 0$ (i.e., without truncation) and $\gamma = 1$ (i.e., no subdiffusion), model (4) reduces to the standard space-fractional advection-diffusion equation

$$\frac{\partial C(x,t)}{\partial x} = -V\frac{\partial C(x,t)}{\partial x} + D\frac{\partial^{\alpha} C(x,t)}{\partial x^{\alpha}}, \tag{5}$$

which is the long-time limit of the CTRW where fast particle motions have a power-law probability density function. The derivation and underlying physical meaning of model (5) were shown for details in the extensive review in [62]. While sampling natural media, solute particles experience various velocity zones. A smaller value of the index α indicates a broader distribution of high velocity zones (ahead of the mean), indicating a more highly heterogeneous medium. Model (5) was used to capture the anomalous transport of conservative tracers through unsaturated soils [49, 59], saturated porous media [11, 27, 63], streams and rivers [31], and overland flow [19]. As a conclusion of the above review, the selection of a single-side space fractional-derivative model has been found physically reasonable for solute transport processes.

The second necessary modification of model (1) is the time drift term added on the left hand side of (1) in order to distinguish the solute particle state (in mobile or immobile phases, see (7)). Such improvement is analogous to the time drift term shown in the composite fractional relaxation equation (see (4.1) in [22]). In some physical processes such as contaminant transport in ground water, the subdiffusive effect due to mass exchange between mobile and relatively immobile phases is almost ubiquitous [24]. The following time-fractional advection-diffusion equation (ADE) models, proposed first by Schumer et al. [56] and applied extensively by hydrologists (see the review in [62]), employ stable waiting times to create a subdiffusive effect:

$$\left(\frac{\partial}{\partial t} + \beta\frac{\partial^{\gamma}}{\partial t^{\gamma}}\right)C_T = -L_x C_T, \tag{6a}$$

$$\left(\frac{\partial}{\partial t} + \beta\frac{\partial^{\gamma}}{\partial t^{\gamma}}\right)C_m = -L_x C_m - \beta\frac{t^{-\gamma}}{\Gamma(1-\gamma)}C_m(x, t=0). \tag{6b}$$

Here C_T and C_m denote the solute concentration in the total (mobile plus immobile) phase and the mobile phase, respectively, β $[T^{\gamma-1}]$ is the fractional capacity coefficient, the scale index γ [dimensionless] $(0 < \gamma < 1)$ controls the power-law distribution of waiting times, Γ is the gamma function, and L_x denotes the advection-diffusion operator. The initial condition $C_m(x, t = 0) > 0$ defines the initial contamination placed only in the mobile zone, to represent typical tracer tests and real-world contamination [56]. Physically, the model (6) assumes a distribution of kinetic rates (first-order reversible kinetic sorption into low velocity zones). A smaller value of the index γ indicates a more strongly heterogeneous set of immobile zones.

If L_x takes the advection-diffusion operator defined in model (4), we obtain the extended and novel TFADE model for the total phase

$$\left(\frac{\partial}{\partial t}+\beta\frac{\partial^\gamma}{\partial t^\gamma}\right)C_T=-V\frac{\partial C_T}{\partial x}+D\left\{e^{-\lambda x}\frac{\partial^\alpha}{\partial x^\alpha}[e^{\lambda x}C_T]-\alpha\lambda^{\alpha-1}\frac{\partial C_T}{\partial x}-\lambda^\alpha C_T\right\}, \tag{7}$$

and the mobile phase

$$\left(\frac{\partial}{\partial t}+\beta\frac{\partial^\gamma}{\partial t^\gamma}\right)C_m=-V\frac{\partial C_m}{\partial x}+D\left\{e^{-\lambda x}\frac{\partial^\alpha}{\partial x^\alpha}[e^{\lambda x}C_m]-\alpha\lambda^{\alpha-1}\frac{\partial C_m}{\partial x}-\lambda^\alpha C_m\right\}$$
$$-\frac{\beta t^{-\gamma}C_m(x,t=0)}{\Gamma(1-\gamma)}. \tag{8}$$

To distinguish from the original TFADE model (1), we name models (7) and (8) as the TFADE-Total and TFADE-Mobile, respectively. When $\alpha=2$, the above extensions reduce to the fractal mobile/immobile model proposed by Schumer et al. [56].

Spatial moments for both models (7) and (8) are derived below. For applications such as ground water sampling in real aquifers, the distinction of particle phases is necessary since samples can be collected preferentially from mobile water [24, 56, 62]. Examples are given in Sect. 5.

3 Spatial Moments for the Extended TFADEs

3.1 The TFADE-Total Model (7)

The solution of (7) in Fourier (k) and Laplace space (s) is

$$\hat{\tilde{C}}_T(k,s)=\frac{1+\beta s^{\gamma-1}}{s+\beta s^\gamma+Vik-D[(\lambda+ik)^\alpha-\lambda^\alpha-ik\alpha\lambda^{\alpha-1}]}\hat{C}_T(k,0), \tag{9}$$

where the symbol hat denotes Fourier transform, and the symbol tilde denotes Laplace transform.

Following the integral transform scheme discussed in Appendix A, we obtain the solute particle mass for model (7) using (9)

$$M_T(t)=\vartheta=\theta_m/\theta_T, \tag{10}$$

where the subscript "T" denotes the total phase, ϑ denotes the initial mass in the total phase, and θ_m and θ_T denotes the effective porosity in the mobile and total phase, respectively. The porosity term appears since we assume that particles are located initially in the mobile phase only (with unit mass).

No exact real-time analytical expressions can be obtained for higher order moments about the origin. Alternatively, we use the asymptotic expansion method to expand the moments about the origin in Laplace space, and then take the inverse Laplace transform to get the approximation in real time. For example, the second-order moment about the origin in Laplace space is

$$\tilde{\mu}_{2,T}(s)=\frac{2V^2\vartheta}{s(s+\beta s^\gamma)^2}+\frac{D\vartheta\alpha(\alpha-1)\lambda^{\alpha-2}}{s(s+\beta s^\gamma)}, \tag{11}$$

where μ denotes the moment about the origin, the first suffix "$_2$" denotes the order of the moment, and the second suffix "$_T$" denotes the total phase. For $|\beta s^{\gamma-1}| < 1$ (or $s > \beta^{\frac{1}{1-\gamma}}$, representing a small real time t_{early}), we can expand (11) to a series representations, which has the following inverse Laplace transform

$$\mu_{2,T}(t_{\text{early}}) \approx 2V^2\vartheta \sum_{n=0}^{N} \frac{(-1)^n(n+1)\beta^n t^{(1-\gamma)n+2}}{\Gamma[(1-\gamma)n+3]} + D\vartheta\alpha(\alpha-1)\lambda^{\alpha-2} \sum_{n=0}^{\infty} \frac{(-1)^n\beta^n t^{(1-\gamma)n+1}}{\Gamma[(1-\gamma)n+2]}. \tag{12}$$

Similarly, for $|(1/\beta)^{\frac{1}{1-\gamma}} s| < 1$ (or $s < \beta^{\frac{1}{1-\gamma}}$, representing a large time t_{late}), we obtain the late-time approximation

$$\mu_{2,T}(t_{\text{late}}) \approx 2V^2\vartheta \sum_{n=0}^{N} (-1)^n(n+1)\beta^{-n-2} \frac{t^{(\gamma-1)n+2\gamma}}{\Gamma[(\gamma-1)n+2\gamma+1]} + D\vartheta\alpha(\alpha-1)\lambda^{\alpha-2} \sum_{n=0}^{\infty} (-1)^n\beta^{-n-1} \frac{t^{(\gamma-1)n+\gamma}}{\Gamma[(\gamma-1)n+\gamma+1]}. \tag{13}$$

The resultant spatial moments higher than the zeroth order therefore have series representations. In the following we show only the dominant terms for each moment, so that their behavior at very small or large time can be evaluated conveniently. The applicability of all these dominant terms will be tested in Sect. 5. The mean displacement grows as

$$E_T(t_{\text{early}}) \approx Vt, \tag{14a}$$

$$E_T(t_{\text{late}}) \approx V\beta^{-1}t^{\gamma}\Gamma_1 \tag{14b}$$

and the variance can be approximated by

$$\sigma_T^2(t_{\text{early}}) \approx D\alpha(\alpha-1)\lambda^{\alpha-2}t, \tag{15a}$$

$$\sigma_T^2(t_{\text{late}}) \approx V^2\beta^{-2}t^{2\gamma}[2\Gamma_2 - (\Gamma_1)^2] + D\alpha(\alpha-1)\lambda^{\alpha-2}\beta^{-1}t^{\gamma}\Gamma_1. \tag{15b}$$

Here $\Gamma_i = 1/\Gamma(i\gamma+1)$ with $i = 1, 2, \ldots$ denotes a factor depending only on γ. The second term on the right hand side (RHS) of (15b) is the dominant term ($n = 0$) of the 2nd series representation in (13). Numerical analysis shows that this term can contribute significantly to $\sigma_T^2(t_{\text{late}})$ if λ is small and t is not reaching infinity.

The skewness of plume in the total phase can be approximated by

$$S_T(t_{\text{early}}) \approx \frac{2-\alpha}{[D\alpha(\alpha-1)]^{1/2}\lambda^{\alpha/2}} t^{-1/2}, \tag{16a}$$

$$S_T(t_{\text{late}}) \approx \left\{V^3\beta^{-3}t^{3\gamma}[6\Gamma_3 - 6\Gamma_2\Gamma_1 + 2(\Gamma_1)^3] + VD\alpha(\alpha-1)\lambda^{\alpha-2}\beta^{-2}t^{2\gamma} \times [6\Gamma_2 - 3(\Gamma_1)^2] - D\alpha(\alpha-1)(\alpha-2)\lambda^{\alpha-3}\beta^{-1}t^{\gamma}\Gamma_1\right\}\left[\sigma_T^2(t_{\text{late}})\right]^{-3/2}, \tag{16b}$$

and the kurtosis of plume in the total phase can be approximated by

$$\kappa_T(t_{\text{early}}) \approx \frac{(\alpha-2)(\alpha-3)}{D\alpha(\alpha-1)\lambda^{\alpha}} t^{-1}, \tag{17a}$$

$$\kappa_T(t_{\text{late}}) \approx \{V^4\beta^{-4}t^{4\gamma}[24\Gamma_4 - 24\Gamma_3\Gamma_1 + 12\Gamma_2(\Gamma_1)^2 - 3(\Gamma_1)^4] + V^2DR\beta^{-3}t^{3\gamma} \times [36\Gamma_3 - 24\Gamma_2\Gamma_1 + 6(\Gamma_1)^3] + \beta^{-2}t^{2\gamma}[(6D^2R^2 - 8VDQ)\Gamma_2 + 4VDQ(\Gamma_1)^2] + QD(\alpha-3)\lambda^{-1}\beta^{-1}t^{\gamma}\Gamma_1\}[\sigma_T^2(t_{\text{late}})]^{-2} - 3, \tag{17b}$$

where $R = \alpha(\alpha-1)\lambda^{\alpha-2}$ and $Q = \alpha(\alpha-1)(\alpha-2)\lambda^{\alpha-3}$.

Note that the early and late time approximations for each moment can also be derived by Karamata's Tauberian theorem [20] (see Appendix B). The early and late time approximations derived in this study have been cross verified by Karamata's theorem.

3.2 The TFADE-Mobile Model (8)

The same asymptotic expansion approach is used to derive the spatial moments for the TFADE-Mobile model (8). The approximated mobile mass M_m decreases in time:

$$M_m(t_{\text{early}}) \approx 1 - \beta t^{1-\gamma}/\Gamma(2-\gamma), \tag{18a}$$

$$M_m(t_{\text{late}}) \approx \beta^{-1}t^{\gamma-1}/\Gamma(\gamma). \tag{18b}$$

The mean displacement E_m grows as

$$E_m(t_{\text{early}}) \approx Vt, \tag{19a}$$

$$E_m(t_{\text{late}}) \approx V\beta^{-1}t^{\gamma}\Gamma_1^*. \tag{19b}$$

where the factor $\Gamma_i^* = \Gamma(\gamma)/\Gamma[(i+1)\gamma]$ (here $i = 1$) is a function of γ.

The variance of mobile phase plume σ_m^2 at the very small and large time increases as

$$\sigma_m^2(t_{\text{early}}) \approx D\alpha(\alpha-1)\lambda^{\alpha-2}t, \tag{20a}$$

$$\sigma_m^2(t_{\text{late}}) \approx V^2\beta^{-2}t^{2\gamma}[2\Gamma_2^* - (\Gamma_1^*)^2] + D\alpha(\alpha-1)\lambda^{\alpha-2}\beta^{-1}t^{\gamma}\Gamma_1^*. \tag{20b}$$

The skewness (S_m) approximation is

$$S_m(t_{\text{early}}) \approx \frac{2-\alpha}{[D\alpha(\alpha-1)]^{1/2}\lambda^{\alpha/2}}t^{-1/2}, \tag{21a}$$

$$S_m(t_{\text{late}}) \approx \{V^3\beta^{-3}t^{3\gamma}[6\Gamma_3^* - 6\Gamma_2^*\Gamma_1^* + 2(\Gamma_1^*)^3] + VD\alpha(\alpha-1)\lambda^{\alpha-2}\beta^{-2}t^{2\gamma} \times [6\Gamma_2^* - 3(\Gamma_1^*)^2] - D\alpha(\alpha-1)(\alpha-2)\lambda^{\alpha-3}\beta^{-1}t^{\gamma}\Gamma_1^*\} \times [\sigma_m^2(t_{\text{late}})]^{-3/2}. \tag{21b}$$

Finally, the Kurtosis κ_m grows as

$$\kappa_m(t_{\text{early}}) \approx \frac{(\alpha-2)(\alpha-3)}{D\alpha(\alpha-1)\lambda^{\alpha}}t^{-1}, \tag{22a}$$

$$\kappa_m(t_{\text{late}}) \approx \{V^4\beta^{-4}t^{4\gamma}[24\Gamma_4^* - 24\Gamma_3^*\Gamma_1^* + 12\Gamma_2^*(\Gamma_1^*)^2 - 3(\Gamma_1^*)^4] + V^2DR\beta^{-3}t^{3\gamma} \times [36\Gamma_3^* - 24\Gamma_2^*\Gamma_1^* + 6(\Gamma_1^*)^3] + \beta^{-2}t^{2\gamma}[(6D^2R^2 - 8VDQ)\Gamma_2^* + 4VDQ(\Gamma_1^*)^2] + QD(\alpha-3)\lambda^{-1}\beta^{-1}t^{\gamma}\Gamma_1^*\}[\sigma_m^2(t_{\text{late}})]^{-2} - 3. \tag{22b}$$

3.3 Discussion

The above moment approximations reveal interesting information about the dynamics of tempered anomalous diffusion. Firstly, we check the similarity and distinction of moments for particles in different phases. At early time, particle plumes captured by either the TFADE-Total model (7) or the TFADE-Mobile model (8) exhibit the same mean, variance, skewness and kurtosis (see for example, (14a) and (19a)). These similarities confirm that most of the particles are in mobile phase at early time, since the initial source is assumed to be in the mobile phase. During this early period, the moments (except for the mass) of the extended TFADEs are also the same as those of (37), a simplified TFADE. At a very small time $t_{\text{early}} < \beta^{\frac{1}{\gamma-1}}$, the contribution of the time-advection term $\partial C/\partial t$ is larger than the time-diffusion term $\beta\partial^\gamma C/\partial t^\gamma$ [56]. Hence the extended models (7) and (8) return roughly to model (37) and generate the same spatial moments. The number $\beta^{\frac{1}{\gamma-1}}$ (with unit $[T]$) provides a rough indication of the time before which the early-time moment approximations in Sects. 3.1 and 3.2 can be used.

When time grows, the loss of mobile particles due to the trapping in the immobile phase is felt gradually by spatial moments, resulting in the subtle difference of moments higher than the zeroth order for solutes in different phases. These moments only differ by their factors Γ_i and Γ_i^*, for plumes in different phases (i.e., comparing (15b) with (20b)). At a late time $t_{\text{late}} \gg \beta^{\frac{1}{\gamma-1}}$, the term $\beta\partial^\gamma C/\partial t^\gamma$ contributes more than the term $\partial C/\partial t$ in the TFADE-Total model (7). Hence the model (7) with $\beta = 1$ reduces to the original TFADE model (1) with $\theta = 1$. This can also be verified by the similarity of their moments. When $\beta = 1$ and $\theta = 1$, the late-time approximations of moments for the TFADE-Total model (7), as expressed by (14b), (15b), (16b) and (17b), are equal to moments for the original TFADE (1) expressed by (36b), (36c), (36d) and (36e), respectively.

Secondly, the above moment formulas show that caution is needed when evaluating the sub- and super-diffusion defined in terms of the second moment. The first and second terms on the RHS of (20b) relate to advection and diffusion, respectively. If the contribution from the advective component dominates and $\gamma > 0.5$, then the transport is superdiffusive (where $\sigma_m^2(t_{\text{late}}) \propto t^{2\gamma}$). If $\gamma < 0.5$, the transport process is always subdiffusive at late time, regardless of the relative contribution of advection and diffusion. In all cases, the mean displacement of solutes always grows slower than the normal diffusion, as shown by (14b) and (19b). It is also noteworthy that, when time $t \to \infty$, the first term on the RHS of (16b), (20b) and (21b) dominates. The skewness therefore approaches to a positive constant. Similar behavior can be found for kurtosis, which approaches to a relatively larger and positive constant. These two constants depend only on γ and are not zero unless $\gamma = 1$. This reveals again the slow convergence of tempered anomalous diffusions to asymptotic diffusion limits.

Finally, we find that the following time-fractional ADE attracts the tempered anomalous diffusion governed by the TFADE-Total model (7) in the long time limit $t \to \infty$

$$\frac{\partial^\gamma C(x,t)}{\partial t^\gamma} = -\frac{V}{\beta}\frac{\partial C(x,t)}{\partial x} + \frac{D\alpha(\alpha-1)\lambda^{\alpha-2}}{2\beta}\frac{\partial^2 C(x,t)}{\partial x^2} + \frac{t^{-\gamma}C_0(x)}{\Gamma(1-\gamma)}. \tag{23}$$

It has the same mean and variance (which have exact analytical expressions) as the late-time approximations of the TFADE-Total model (7). By comparing the skewness approximation (17b) with the analytic skewness for the limit model (23), we find that the crossover time τ_c from the tempered anomalous diffusion to its asymptotic limit scales as $\tau_c \sim \beta^{\frac{1}{\gamma}}\lambda^{-\frac{\alpha}{\gamma}}D^{-\frac{1}{\gamma}}$. When $\beta = 1$, (23) also attracts the tempered process defined by the original TFADE (1) with the maximum skewness coefficient as time goes to infinity.

It is also noteworthy that the extended TFADEs (7) and (8) themselves may be lack of ergodicity, while the standard fractional-order advection-diffusion equation (without tempering) was found to be ergodic by Schumer et al. [55]. A stochastic process is "ergodic" if the distribution of the underlying random walk reaches some limit that does not depend on its initial conditions [20]. For a standard FADE, the ergodic condition is assumed to be produced by plume evolution following any one of the many limiting, stable distributions. Strict mathematical arguments, however, remain to be shown for the standard FADE, where the central limit theory may be used. The standard FADE with variable coefficients can be approximated by a Markov process, as shown for example by Zhang et al. [60]. The ergodicity can be reached only if the underlying diffusion process (i.e., solution to the stochastic differential equation $dx(t) = a(x)dt + b(x)dB(t)$, where $a(x)$ denotes the local drift, $b(x)$ is a function defining the dispersion strength, and $dB(t)$ is a standard Lévy stable noise) can converge to a constant coefficient FADE. Additional arguments are needed for the tempered FADE models. For example, both the statistics of parameters $a(x)$ and $b(x)$ and the scaling leading to the tempered stable remain to be shown. This topic is beyond the scope of this work and will be the focus of a future study.

4 Numerical Solution of Spatial Moments for the TFADE Models

Exact analytical expressions and series representations derived above reveal clearly the evolution of spatial moments in time. In real applications, however, more complex initial and/or boundary conditions can appear, which are beyond the capabilities of analytical or approximation methods. In addition, the approximation of moments for the extended TFADE models developed in Sect. 3 does not cover the whole time period. The intermediate behavior of moments may be important for real physical processes. The two limitations motivate the development of numerical solutions of moments.

The fractional-order partial differential equations were solved by various numerical methods in the last decade, see the review by Zhang et al. [61] and references cited therein. The fully Lagrangian approach is relatively new [13, 23, 30, 36], but it is the only viable tool for solving vector FPDEs with a general mixing measure [61]. To approximate simultaneously the solutions of the two extended TFADE models (7) and (8), we build the following four-step Lagrangian scheme.

Step 1 Decompose the TFADE-Total model (7) into a hitting time process

$$\frac{\partial h(\tau,t)}{\partial \tau} = -\frac{\partial}{\partial t}h(\tau,t) - \beta\frac{\partial^{\gamma}}{\partial t^{\gamma}}h(\tau,t) \tag{24}$$

and a motion process

$$\frac{\partial}{\partial \tau}u(x,\tau) = -V\frac{\partial u(x,\tau)}{\partial x} + D\left\{e^{-\lambda x}\frac{\partial^{\alpha}}{\partial x^{\alpha}}[e^{\lambda x}u(x,\tau)] - \alpha\lambda^{\alpha-1}\frac{\partial u(x,\tau)}{\partial x} - \lambda^{\alpha}u(x,\tau)\right\}, \tag{25}$$

following the argument in [61]. The initial condition for the hitting time process (24) is $h(\tau = 0, t) = \delta(t) + \beta\, t^{-\gamma}/\Gamma(1-\gamma)$. Here τ [T] is the operational or mobile time, and t [T] is the real or clock time.

Step 2 Solve the hitting time process (24) to transfer τ to t. Following the argument in Zhang et al. [61], we derive the generalized Markovian process in the domain of real time t

$$dT_i = a_1 d\tau_i + a_2 \left[\beta \cos\frac{\pi\gamma}{2} d\tau_i\right]^{1/\gamma} S_i(\beta^* = +1,\ \sigma^* = 1,\ \mu^\star = 0, \gamma), \tag{26}$$

where dT_i is the total time spent by the particle during the i-th jump, $d\tau_i$ is the mobile time step, and S_i is a standard γ-stable random variable (with skewness $\beta^* = +1$, scale $\sigma^* = 1$, and shift $\mu^\star = 0$). The two factors a_1 and a_2 enhance the flexibility of the Lagrangian solver. When $a_1 = a_2 = 1$, the solver is for the extended TFADE models (7) and (8). When $a_1 = 0$ and $a_2 = 1$, it solves the time fractional ADE (23). When $a_1 = 1$ and $a_2 = 0$, it solves the simplified TFADE (37) derived by Baeumer and Meerschaert [2]. Note that the first term on the RHS of (26) represents the motion time, while the second term denotes the waiting time. The real time t_i hence can be calculated by

$$t_i = \sum_{j=1}^{i} dT_j. \tag{27}$$

Step 3 Calculate the jump size at each time step by solving the motion process (25). The corresponding particle movement at the i-th jump contains a drift term and a truncated diffusion length, which can be written as

$$dX_i = (V + D\alpha\lambda^{\alpha-1}) d\tau_i + d\xi_i, \tag{28}$$

where the term $D\alpha\lambda^{\alpha-1} d\tau_i$ corrects the mean displacement due to the truncation of α-stable Lévy distribution. The noise $d\xi_i$ can be generated using the exponential rejection method proposed by Baeumer and Meerschaert [2]. Particularly, one can calculate $d\xi_i$ using

$$d\xi_i = \left[-\cos\frac{\pi\alpha}{2} D d\tau_i\right]^{1/\alpha} S_i(\beta^* = +1, \sigma^* = 1, \mu = 0,\ \alpha). \tag{29}$$

Then the value of $d\xi_i$ needs to be evaluated by the criterion

$$d\xi_i \le \mathrm{Exp}_i, \tag{30}$$

where Exp_i is an exponentially distributed random variable with mean $1/\lambda$ (inverse of the truncation parameter), and it can be generated by

$$\mathrm{Exp}_i = -\frac{\ln(U_i)}{\lambda}, \tag{31}$$

where U_i is distributed uniformly on (0, 1). If $d\xi_i > \mathrm{Exp}_i$, then we reject it and re-generate $d\xi_i$ using (29) and Exp_i using (31), until the criterion (30) is met.

Step 4 Calculate the particle position Y at real time t_i via the relationship

$$Y(t_i) = \sum_{j=1}^{i} dX_j. \tag{32}$$

The distinction between the mobile and immobile states for each particle is convenient. For the time between dT_{i-1} and $dT_{i-1} + d\tau_i$ (where dT_{i-1} is the time at the last jump), the

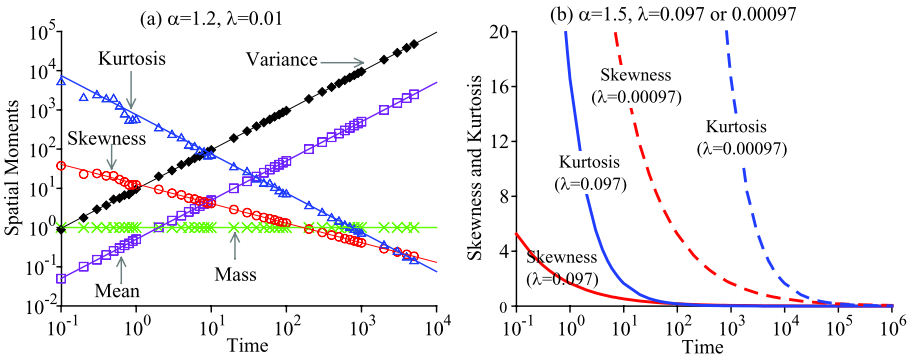

Fig. 1 (**a**) Lagrangian solutions (*symbols*) versus the analytical solutions (*lines*) of moments for the simplified TFADE model (37). Model parameters are: $\alpha = 1.2$, $\lambda = 0.01$, $V = 0.5$, $D = 1$, and $\lambda = 0.01$. (**b**) Convergence speed of skewness and kurtosis due to the truncation parameter λ

particle is in motion; for the remaining time (from $dT_{i-1} + d\tau_i$ to dT_i), the particle is in the immobile state. Hence the two equations (7) and (8) can be solved during one simulation.

To cross verify the above Lagrangian scheme, an implicit Eulerian finite difference solver is also developed (see Appendix C). See Appendix C and the next section for verification of the above Lagrangian scheme. After the TFADEs are solved, spatial moments can be calculated easily given the spatiotemporal distribution of particles.

5 Numerical Examples and Field Applications

5.1 Numerical Examples

We first check the Lagrangian numerical results against the analytical solutions of moments for the simplified TFADE model (37) derived in Appendix A. One example is shown in Fig. 1a, where the Lagrangian solution generally matches the analytical solution (38). The positive values of high order moments, including skewness and kurtosis, exhibit the slow and smooth convergence of the tempered anomalous diffusion to Gaussian statistics. Figure 1b shows that the truncation parameter λ affects significantly the rate of transition from anomalous diffusion to asymptotic diffusion limit. As λ gets larger (and α and D remain unchanged), the anomalous large jumps decrease and therefore the transition from anomalous to normal diffusion is relatively faster.

The next example (Fig. 2) shows moments for the extended TFADE model (7). The Lagrangian approach provides the full time evolution of spatial moments, where the early and late time portions generally match the series representations derived in Sect. 3. Analytical solutions of moments for the asymptotic diffusion equation (23) are also shown for comparison (see the dashed lines in Fig. 2). Eventually, the moments of (7) should converge to the dashed lines, while the truncation parameter λ affects the convergence speed. Because $\beta = 1$ in this example, the early-time approximations derived in Sect. 3 are valid for $t < \beta^{\frac{1}{\gamma-1}} = 1$. On the other hand, the late-time approximations are generally valid at a large time $t \gg \beta^{\frac{1}{\gamma-1}}$.

Finally, we check the moments for particles in different phases, where the particle dynamics is governed by the TFADE-Total model (7) and the TFADE-Mobile model (8), respectively. The mobile-phase plume has similar moments as the plume in the total phase at

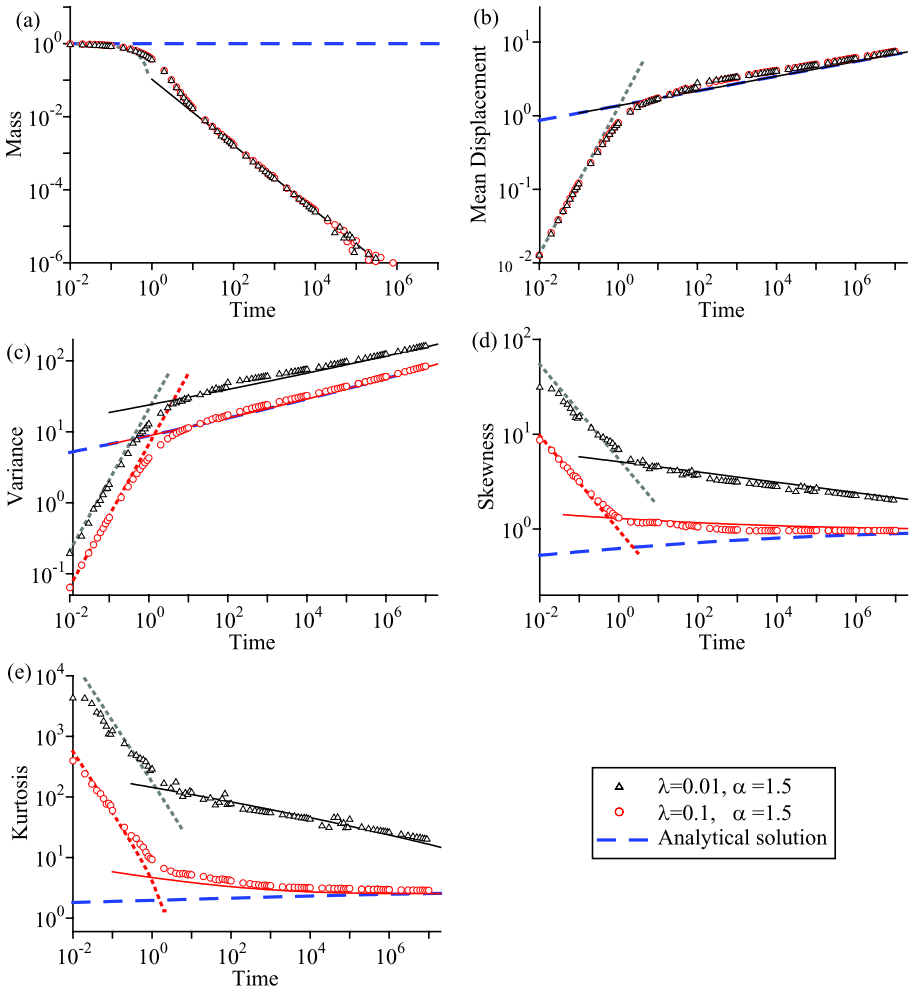

Fig. 2 Lagrangian solutions (*symbols*) versus the series representations (*dots* or *solid lines*) of spatial moments for the TFADE-Total model (7) (except for the mobile mass, which is the solution of TFADE-Mobile (8) for the mobile phase). The *dotted* and *solid lines* are series representations at early and late times, respectively. Model parameters are: $\alpha = 1.5$, $\gamma = 0.1$, $\beta = 1$, $V = 1.3$, $D = 2.8$, and $\lambda = 0.1$ (*circles*) and 0.01 (*triangles*), respectively. Analytical solutions of moments for (23) are also shown (*dashed lines*) for comparison

early time (Fig. 3). Then the mobile mass declines apparently, and the mobile-phase plume moves relatively faster downstream (than the particles in the immobile phase) and separates gradually from the plume trapped in the immobile zones (see also Fig. 9b in Appendix C). Therefore, at late times, the mobile-phase plume has a relatively larger mean and variance for displacement, and a relatively smaller skewness and kurtosis, than those of the total-phase plume. This is consistent with the series representations derived in Sect. 3.

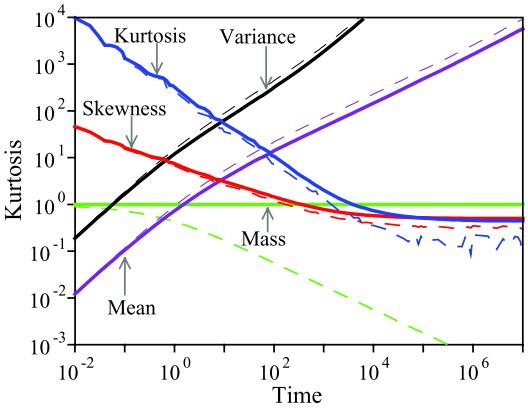

Fig. 3 Lagrangian solutions of the spatial moments for the TFADE-Total model (7) (total phase, *solid lines*) and the TFADE-Mobile model (8) (mobile phase, *dashed lines*). Model parameters are: $\alpha = 1.5$, $\gamma = 0.5$, $\beta = 1$, $V = 1.3$, $D = 2.8$, and $\lambda = 0.01$. Note the initial mass is 1

5.2 Field Application 1—MADE Site

Contaminant transport through porous media can experience the transition from anomalous diffusion to local limits, as shown by the pioneering work in the fluid mechanics community (see for example [16, 17, 48]). This motivated us to apply the TFADE model to capture real transport processes in natural porous media. Natural gradient tracer (bromide) tests conducted at the MAcroDispersion Experiments (MADE) at Columbus, MS [1, 3, 4, 51], one of the most intensively studied sites in North America, exhibit complex diffusion in the highly heterogeneous alluvial aquifer/aquitard system. For almost two decades, the hydrology community has developed numerous numerical models and various transport theories to explain the MADE-site bromide plumes (see the extensive review in [62]), but the efficient transport model that can capture the measured spatial moments is rather limited. We find that the measured spatial moments (Fig. 4) favor the application of the TFADE-Mobile model (8). For example, the mobile mass data (Fig. 4a) declines as power-law when time increases, matching the trend revealed by formula (18b). The mean displacement of solutes increases slower than linear, suggesting also the subdiffusive effect due to the trapping in aquitards (see also (19b)). The plume variance evolves irregularly in time, where the noise is probably due to the irregular variation of detection length at different sampling cycles [1]. Finally, the skewness and kurtosis are much larger than zero, suggesting persistent preasymptotic transport behavior that can be captured by the TFADE model. Geological data also support the application of a tempered Lévy motion model. For example, the distribution of the measured hydraulic conductivity (K) transitions from power-law to exponential (Fig. 5), implying that the MADE site may not have infinite velocity or a purely power-law distributed solute movement.

The above measurements motivated the application of the TFADE-Mobile model (8) to fit the moment data. The numerical approach is needed to incorporate the influence of limited detection lengths on spatial moments. First, bromide mass fraction (Fig. 4a) is fitted to obtain the parameters γ (which is 0.35) and β (0.08 day$^{-0.65}$) (as revealed by (18)). Next, the fit of the mean displacement of plumes provides velocity V ($= 0.17$ m/day), which follows the field measurements ($0.12 < V < 0.36$ m/day). Finally, the fit of the plume variance (Fig. 4c) provides the diffusion coefficient D (0.35 m$^{\alpha}$/day) and the truncation parameter λ (0.005 m^{-1}). The index α (1.1) can be fitted by either the variance data, or the distribution of K (the details for latter can be found in [62]). Hence all parameters in model (8) can be fitted based on the first three moments, leaving the skewness and kurtosis measurements

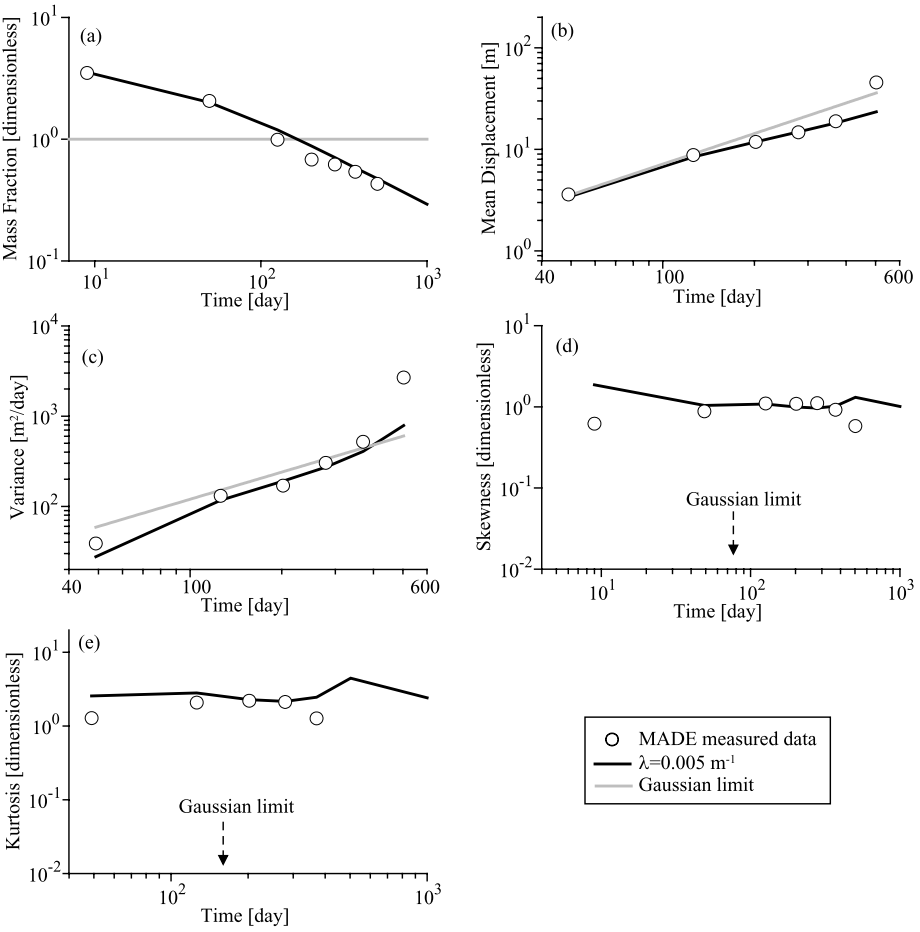

Fig. 4 The best-fit moments (the *black line*) using the TFADE-Mobile (8) versus the measured moments (*circles*) at the MADE site. The initial mass is 5, based on Harvey and Gorelick [25]. The *grey line* denotes the best-fit of the classical 2nd-order ADE, where both the skewness and kurtosis are 0

as verification targets (Fig. 4d, e). Note the classical 2nd-order ADE can also be fitted by the measured mean and variance (see the grey line in Fig. 4b, c), but it underestimates significantly the skewness and kurtosis. Also note that the sampling cycles of this experiment ($10 \sim 500$ days) are around the specific time $\beta^{\frac{1}{\gamma-1}} = 49$ days, an intermediate period that requires the numerical solver for moment calculation.

Model (8) with the best-fit parameters is further applied to check against the observed plume snapshots (Fig. 6). We also test the influence of λ on the leading edge of bromide plumes. A relatively large λ tends to underestimate the leading edge of bromide plumes.

5.3 Field Application 2—Cape Cod Site

Bromide transport has also been monitored during a natural gradient tracer test conducted at the well-known Cape Cod site, Massachusetts [21, 35]. Glaciofluvial deposits with stratified sand/gravel and minor silt/clay form the unconfined aquifer. The $\ln(K)$ variance is as small

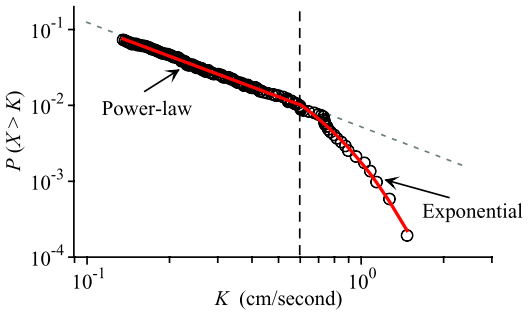

Fig. 5 The measured (*circle*) and the best-fit (*solid line*) hydraulic conductivity (K) distribution at the MADE site

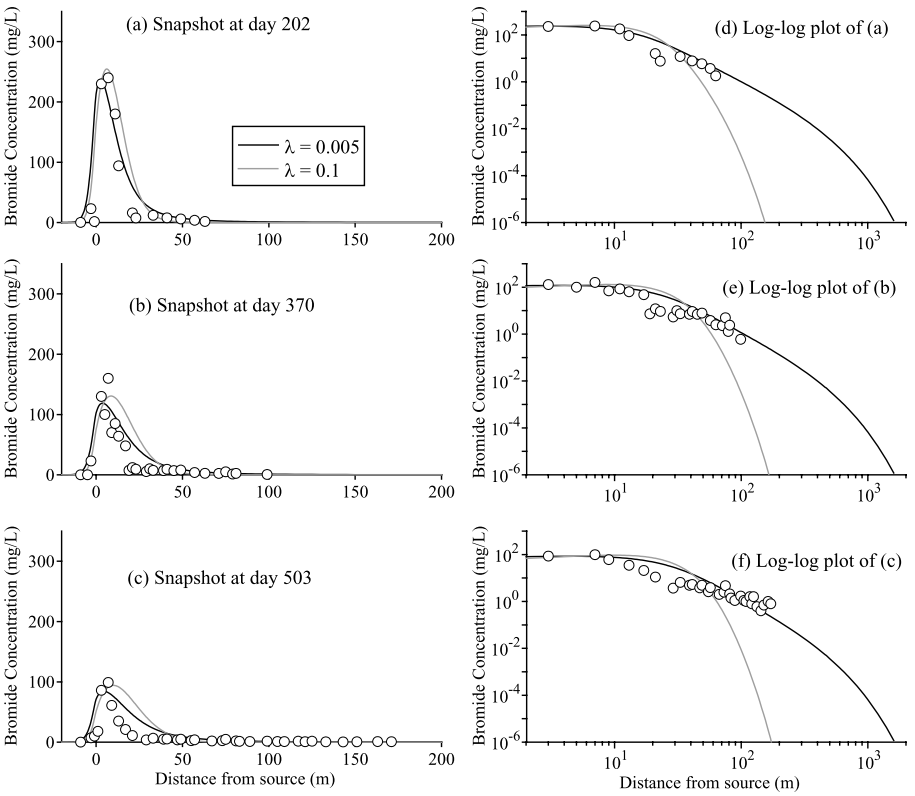

Fig. 6 Predicted (*black lines* with $\lambda = 0.005$) (using model (8) and parameters fitted in Fig. 4) versus measured (*symbols*) bromide concentrations from the MADE site at the sampling cycle at day 202 (**a**), 370 (**b**), and 503 (**c**), respectively. (**d**), (**e**), and (**f**) are the log-log plot of (**a**), (**b**), and (**c**), respectively. The unit of λ is m^{-1}. A much larger $\lambda = 0.1$ is also shown for comparison

as 0.26, representing an end-member ("homogeneous") of alluvial systems, compared to the heterogeneous MADE site (where the variance of $\ln(K)$ is 4.5). The first three moments were measured (Fig. 7), and the best-fit parameters using model (8) are: $\gamma = 0.90$, $\beta = 0.01$ day$^{-0.1}$, $V = 0.45$ m/day, $\alpha = 1.95$, $D = 0.3$ m$^{1.95}$/day, and a relatively large truncation parameter $\lambda = 0.02$ m^{-1}. The best-fit velocity is within the range of field measurements

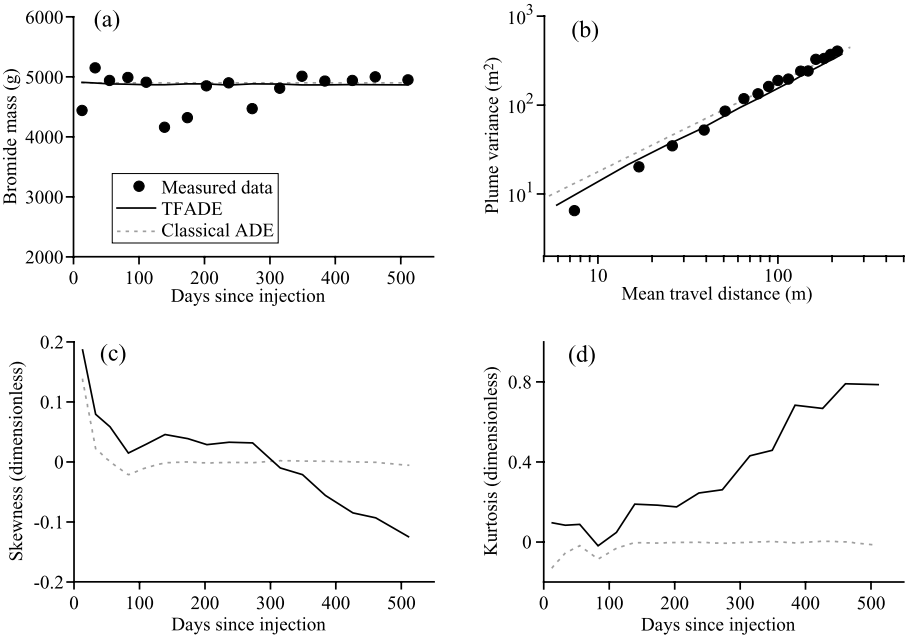

Fig. 7 Measured (*symbols*) versus fitted Cape Cod Bromide spatial moments (zeroth to the second orders) using the TFADE-Mobile model (8). (**a**) mass, (**b**) mean travel distance versus the variance of displacement. Solutions of the classical 2nd-order ADE are added for comparison. In (**a**), the best-fit mobile mass using (8) is almost identical to the solution of the classical 2nd-order ADE. (**c**) and (**d**) show the predicted skewness and kurtosis, respectively, where there were no measured data. Note the noise of moments in (**c**) and (**d**) at early time (<90 days) is due to the irregular detection length

(0.39 ∼ 0.51 m/day [21]). There are no measurements for skewness and kurtosis, and we only list predictions in Fig. 7c, d.

The homogeneous nature of Cape Cod deposits generates relatively "weak" anomalous diffusion, as shown by the first three integer order moments. The measurement noise in mobile mass conceals any possible decrease of mass. The mean and variance of plumes can also be fitted reasonably well by the classical 2nd-order ADE. The higher order moments including skewness and kurtosis, however, distinguish clearly the anomalous nature from Gaussian statistics (see Fig. 7c, d).

Further prediction of the bromide plume shows the superiority of the TFADE-Mobile model (8) over the classical ADE (Fig. 8). The leading and trailing tails of bromide plumes are apparently heavier than the ones predicted by a Gaussian model, confirming the large kurtosis predicted by model (8) and shown in Fig. 7d.

The above applications support the exponential truncation of Lévy process. There are other ways to temper a Lévy stable density, such as the power-law truncation [15, 57], the damped Lévy flights (Lévy flights in velocity (phase) space with non-linear friction) [14], and the confined Lévy flights (i.e., the flights in potential wells, see [12, 13]). Rosiński [52] also showed that, tempered stable distributions admit parametrization similar to stable distributions, and the change of measure on the probability space results in a large class of tempered stable Lévy processes. We will compare the truncation of these physical models to actual truncation observed in hydrology problems in a future study.

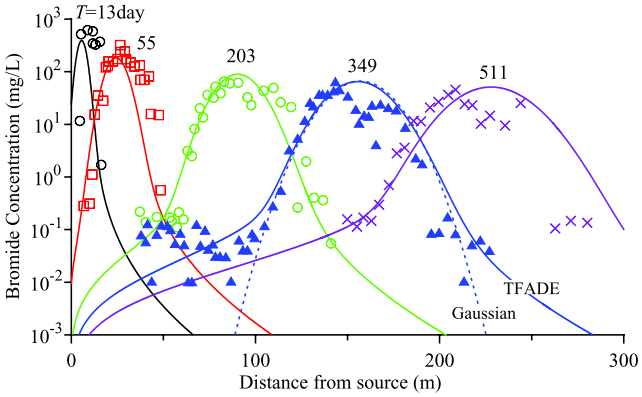

Fig. 8 The measured (*symbols*) versus the predicted (*lines*) Cape Cod bromide snapshots using the TFADE-Mobile model (8). Model parameters are fitted in Fig. 7. The classical 2nd-order ADE solution at day 349 (*dots*) is also listed for comparison

6 Conclusion

Moment formulas are developed for exponentially tempered fractional advection-diffusion equations. Exact analytical expression can be derived for moments for the original TFADE model by using the standard, integral transform approach. The extended TFADE models that capture also the subdiffusive effect have no analytical solutions for moments, but the series representations of moments can be derived using the asymptotic expansion method.

The derived moments reveal interesting information of tempered anomalous diffusion, such as the diffusion equation that attracts the tempered anomalous diffusion in the long time limit. They also help to analyze the early/late time behavior of preasymptotic transport in different phases and the scale of crossover time for asymptotic diffusion to appear, improving the understanding of tempered anomalous diffusion appearing in a complex environment.

Numerical approaches are needed to explore spatial moments if the full time evolution of moments is desirable, or the diffusive process contains complex initial/boundary conditions. Applications in two end-members of alluvial settings show the importance of high order moments including skewness and kurtosis, in distinguishing preasymptotic transport from asymptotic diffusion limits. In particular, the truncation parameter λ increases with the decrease of the variance of hydraulic conductivity, implying a potential link between system heterogeneity and the tempered stable Lévy process.

Acknowledgements The work was supported by the National Science Foundation (NSF) under EAR-0748953 and Desert Research Institute (DRI). This paper does not necessary reflect the view of the NSF or DRI. Y.Z. also thanks Mark M. Meerschaert, Boris Baeumer and two anonymous reviewers for helpful remarks that improved the manuscript.

Appendix A: Analytical Solution of Moments for the Original TFADE Model (1)

The analytic solution of the evolution of moments up to the fourth-order for the original TFADE model (1) is derived here using the integral (Laplace-Fourier) transform approach.

Taking the Fourier transform ($x \to k$) and Laplace transform ($t \to s$) of the original FPDE (1), we get the solution for P

$$\hat{\tilde{P}}(k,s) = \frac{s^{\gamma-1}}{s^\gamma + Vik - D[l(\lambda+ik)^\alpha + r(\lambda-ik)^\alpha - \lambda^\alpha - ik\alpha\lambda^{\alpha-1}\theta]}\hat{P}(k,0), \tag{33}$$

where $\hat{\tilde{P}}$ is both the Fourier transform and the characteristic function of P, and $\hat{P}(k,0)$ is the initial density. The n-th order moment about the origin of P, denoted as μ_n, is related to $\hat{P}$ via:

$$\left.\frac{d^n \hat{\tilde{P}}(k,s)}{dk^n}\right|_{k=0} = (-i)^n \tilde{\mu}_n(s). \tag{34}$$

Note here the Laplace transform and its inverse operation are not needed if the Fourier transform itself can solve the differential equation. Combining (33) and (34) and taking inverse Laplace transform, we obtain the zeroth-order to fourth-order moments about the origin in real time:

$$\mu_0(t) = 1, \tag{35a}$$

$$\mu_1(t) = \frac{Vt^\gamma}{\Gamma(\gamma+1)}, \tag{35b}$$

$$\mu_2(t) = \frac{2V^2t^{2\gamma}}{\Gamma(2\gamma+1)} + \frac{D\alpha(\alpha-1)\lambda^{\alpha-2}t^\gamma}{\Gamma(\gamma+1)}, \tag{35c}$$

$$\mu_3(t) = \frac{6V^3t^{3\gamma}}{\Gamma(3\gamma+1)} + \frac{6VD\alpha(\alpha-1)\lambda^{\alpha-2}t^{2\gamma}}{\Gamma(2\gamma+1)} - \frac{D\alpha(\alpha-1)(\alpha-2)\lambda^{\alpha-3}\theta t^\gamma}{\Gamma(\gamma+1)}, \tag{35d}$$

$$\mu_4(t) = \frac{24V^4t^{4\gamma}}{\Gamma(4\gamma+1)} + \frac{36V^2D\alpha(\alpha-1)\lambda^{\alpha-2}t^{3\gamma}}{\Gamma(3\gamma+1)} + \frac{b_1t^{2\gamma}}{\Gamma(2\gamma+1)} + \frac{b_2t^\gamma}{\Gamma(\gamma+1)}, \tag{35e}$$

where the parameter $b_1 = 6[D\alpha(\alpha-1)\lambda^{\alpha-2}]^2 - 8VD\alpha(\alpha-1)(\alpha-2)\lambda^{\alpha-3}\theta$ and $b_2 = D\alpha(\alpha-1)(\alpha-2)(\alpha-3)\lambda^{\alpha-4}$. Here we assume that (1) the initial mass is 1 (i.e., normalization), and (2) there is no other source or sink in the system.

Spatial moments can then be derived given the relationship between central moments and moments about the origin. Hence we obtain the particle total mass M, mean E and variance σ^2 of particle displacements, skewness S and kurtosis κ (note M and E are equal to the zeroth-order and first-order moments around the origin, respectively):

$$M(t) = 1, \tag{36a}$$

$$E(t) = \frac{Vt^\gamma}{\Gamma(\gamma+1)}, \tag{36b}$$

$$\sigma^2(t) = V^2t^{2\gamma}\left[\frac{2}{\Gamma(2\gamma+1)} - \frac{1}{(\Gamma(\gamma+1))^2}\right] + \frac{D\alpha(\alpha-1)\lambda^{\alpha-2}t^\gamma}{\Gamma(\gamma+1)}, \tag{36c}$$

$$S(t) = \left\{V^3t^{3\gamma}\left[\frac{6}{\Gamma(3\gamma+1)} - \frac{6}{\Gamma(2\gamma+1)\Gamma(\gamma+1)} + \frac{2}{(\Gamma(\gamma+1))^3}\right]\right.$$
$$\left. + VD\alpha(\alpha-1)\lambda^{\alpha-2}t^{2\gamma}\left[\frac{6}{\Gamma(2\gamma+1)} - \frac{3}{(\Gamma(\gamma+1))^2}\right]\right.$$

$$- D\alpha(\alpha-1)(\alpha-2)\lambda^{\alpha-3}\theta t^{\gamma}\frac{1}{\Gamma(\gamma+1)}\Bigg\}[\sigma^2(t)]^{-3/2} \tag{36d}$$

$$\begin{aligned}\kappa(t) = \Bigg\{ & V^4 t^{4\gamma}\left[\frac{24}{\Gamma(4\gamma+1)} - \frac{24}{\Gamma(3\gamma+1)\Gamma(\gamma+1)} + \frac{12}{\Gamma(2\gamma+1)(\Gamma(\gamma+1))^2}\right.\\ & \left. - \frac{3}{(\Gamma(\gamma+1))^4}\right] + V^2 D\alpha(\alpha-1)\lambda^{\alpha-2}t^{3\gamma}\left[\frac{36}{\Gamma(3\gamma+1)} - \frac{24}{\Gamma(2\gamma+1)\Gamma(\gamma+1)}\right.\\ & \left. + \frac{6}{(\Gamma(\gamma+1))^3}\right] + D\alpha(\alpha-1)\lambda^{\alpha-2}t^{2\gamma}\left[\frac{6D\alpha(\alpha-1)\lambda^{\alpha-2}}{\Gamma(2\gamma+1)} - \frac{8V(\alpha-2)\lambda^{-1}\theta}{\Gamma(2\gamma+1)}\right.\\ & \left. - \frac{4V(\alpha-2)\lambda^{-1}\theta}{(\Gamma(\gamma+1))^2}\right] - \frac{D\alpha(\alpha-1)(\alpha-2)(\alpha-3)\lambda^{\alpha-4}t^{\gamma}}{\Gamma(\gamma+1)}\Bigg\}[\sigma^2(t)]^{-2} - 3. \end{aligned} \tag{36e}$$

Formula (36b) shows that the truncation of large jumps does not alter the mean shift, since the tempered stable Lévy motion has a mean zero (captured by the term $D\alpha\lambda^{\alpha-1}\partial P/\partial x$ in model (1)). The mean and variance shown by (36b) and (36c) are consistent to the ones provided by Cartea and del-Castillo-Negrete [10]. Also note that the skewness coefficient θ affects only the moments higher than the second order.

When $\gamma = 1$ and $\theta = 1$, the original TFADE (1) reduces to the simplified TFADE derived by Baeumer and Meerschaert [2]:

$$\frac{\partial P(x,t)}{\partial t} = -V\frac{\partial P(x,t)}{\partial x} + D\left\{e^{-\lambda x}\frac{\partial^{\alpha}[e^{\lambda x}P(x,t)]}{\partial x^{\alpha}} - \alpha\lambda^{\alpha-1}\frac{\partial P(x,t)}{\partial x} - \lambda^{\alpha}P(x,t)\right\}, \tag{37}$$

which contains only the space fractional derivative. The corresponding moments (36) reduce to

$$M(t) = 1, \tag{38a}$$

$$E(t) = Vt, \tag{38b}$$

$$\sigma^2(t) = D\alpha(\alpha-1)\lambda^{\alpha-2}t, \tag{38c}$$

$$S(t) = \frac{2-\alpha}{[D\alpha(\alpha-1)]^{1/2}\lambda^{\alpha/2}}t^{-\frac{1}{2}}, \tag{38d}$$

$$\kappa(t) = \frac{(\alpha-2)(\alpha-3)}{D\alpha(\alpha-1)\lambda^{\alpha}}t^{-1}. \tag{38e}$$

For this simplified TFADE, the variance increases linearly with time, just as any other Lévy process with finite second moment. This is because X_t is the sum of t independent and identically distributed random variables, and variances of independent random variables add. A similar formula $\sigma^2(t) \sim D\lambda^{\alpha-2}t$ was found by Koponen [33]. The higher order moments, including skewness and kurtosis, distinguish the preasymptotic diffusion from normal diffusion. Here the skewness decreases as $t^{-1/2}$, while the kurtosis decreases relatively faster. The rate at which the two moments approach zero reflects the speed at which tempered anomalous diffusion converges to normal diffusion. In particular, formulas (38d) and (38e) show that the combination of D, α and λ affects the rate of convergence. Only when $t \gg \frac{(2-\alpha)}{\alpha(\alpha-1)}D^{-1}\lambda^{-\alpha}$ will the skewness and kurtosis be small enough to approximate Gaussian statistics. This is consistent with the conclusion obtained by Del-Castillo-Negrete [18], who showed that the crossover time τ_c for Gaussian behavior to appear scales as $\tau_c \sim D^{-1}\lambda^{-\alpha}$.

When $t \to \infty$, model (37) is asymptotically Gaussian, and the corresponding formula (38) reduces to the moments for the classical 2nd-order advection-diffusion equation

$$\frac{\partial C(x,t)}{\partial t} = -V\frac{\partial C(x,t)}{\partial x} + \frac{1}{2}D\alpha(\alpha-1)\lambda^{\alpha-2}\frac{\partial^2 C}{\partial x^2}. \tag{39}$$

It identifies the classical diffusion equation that attracts the tempered anomalous diffusion in the long time limit.

Appendix B: Tauberian Theorem to Derive the Early and Late Time Approximations of Moments for the Extended TFADE

As an illustration, Karamata's Tauberian theorem [20] is applied here to derive the early and late time approximations for variance for the TFADE-Total model (7).

Denote $\mu_{2,T}(t)$ as the second-order moment about the origin in real time. The following integral defines a new function $W(t)$

$$W(t) = \int_0^t \mu_{2,T}(r)dr. \tag{40}$$

Karamata's theorem (see Theorem 3, p. 445 in [20]) shows that

$$\tilde{\mu}_{2,T}(s) \sim Bs^{-\xi} \quad \text{as } s \to 0 \quad \Longleftrightarrow \quad W(t) \sim \frac{Bt^{\xi}}{\Gamma(\xi+1)} \quad \text{as } t \to \infty, \tag{41}$$

where the parameter $B > 0$, $\xi \geq 0$, and the symbol "$\sim$" between two functions means that the ratio $f_1/f_2 \to 1$ (where f_1 and f_2 denote the function before and after "$\sim$", respectively).

Based on (11), one can write

$$\begin{aligned}\tilde{\mu}_{2,T}(s) &= \frac{2V^2\vartheta}{s(s+\beta s^{\gamma})^2} + \frac{D\vartheta\alpha(\alpha-1)\lambda^{\alpha-2}}{s(s+\beta s^{\gamma})} \\ &= \frac{2V^2\vartheta}{\beta^2 s^{2\gamma+1}(\beta^{-1}s^{1-\gamma}+1)^2} + \frac{D\vartheta\alpha(\alpha-1)\lambda^{\alpha-2}}{\beta s^{\gamma+1}(\beta^{-1}s^{1-\gamma}+1)} \\ &\sim \frac{2V^2\vartheta}{\beta^2}s^{-(2\gamma+1)} + \frac{D\vartheta\alpha(\alpha-1)\lambda^{\alpha-2}}{\beta}s^{-(\gamma+1)}\end{aligned} \tag{42}$$

as $s \to 0$. The statement (41) shows that

$$W(t) \sim \frac{2V^2\vartheta}{\beta^2}\frac{t^{2\gamma+1}}{\Gamma(2\gamma+2)} + \frac{D\vartheta\alpha(\alpha-1)\lambda^{\alpha-2}}{\beta}\frac{t^{\gamma+1}}{\Gamma(\gamma+2)} \quad \text{as } t \to \infty. \tag{43}$$

Hence the late time approximation for $\mu_{2,T}(t)$ is

$$\mu_{2,T}(t) = \frac{dW(t)}{dt} \sim \frac{2V^2\vartheta}{\beta^2}\frac{t^{2\gamma}}{\Gamma(2\gamma+1)} + \frac{D\vartheta\alpha(\alpha-1)\lambda^{\alpha-2}}{\beta}\frac{t^{\gamma}}{\Gamma(\gamma+1)} \quad \text{as } t \to \infty. \tag{44}$$

To derive the early time approximation for $\mu_{2,T}(t)$, another version of Karamata's theorem is needed:

$$\tilde{\mu}_{2,T}(s) \sim Bs^{-\xi} \quad \text{as } s \to \infty \quad \Longleftrightarrow \quad W(t) \sim \frac{Bt^{\xi}}{\Gamma(\xi+1)} \quad \text{as } t \to 0. \tag{45}$$

We can rewrite (11):

$$\tilde{\mu}_{2,T}(s) = \frac{2V^2\vartheta}{s^3(1+\beta s^{\gamma-1})^2} + \frac{D\vartheta\alpha(\alpha-1)\lambda^{\alpha-2}}{s^2(1+\beta s^{\gamma-1})}$$
$$\sim 2V^2\vartheta\, s^{-3} + D\vartheta\alpha(\alpha-1)\lambda^{\alpha-2}s^{-2} \tag{46}$$

as $s \to \infty$. The theory (45) gives $W(t)$

$$W(t) \sim V^2\vartheta\frac{t^3}{3} + D\vartheta\alpha(\alpha-1)\lambda^{\alpha-2}\frac{t^2}{2} \quad \text{as } t \to 0. \tag{47}$$

The early time approximation for $\mu_{2,T}(t)$ therefore is

$$\mu_{2,T}(t) \sim V^2\vartheta t^2 + D\vartheta\alpha(\alpha-1)\lambda^{\alpha-2}t \quad \text{as } t \to 0. \tag{48}$$

Following the same procedure from (40) to (48), one can derive that

$$\mu_{1,T}(t) \sim V\vartheta t \quad \text{as } t \to 0, \tag{49a}$$

$$\mu_{1,T}(t) \sim V\vartheta\beta^{-1}t^{\gamma}\frac{1}{\Gamma(\gamma+1)} \quad \text{as } t \to \infty. \tag{49b}$$

Formula (10) reveals that

$$\mu_{0,T}(t) = \vartheta, \tag{50}$$

which is an exact solution valid for all t. By combining (48), (49a) and (50), the early time approximation for variance for the TFADE-Total model (7) is then obtained

$$\sigma_T^2(t) \sim D\alpha(\alpha-1)\lambda^{\alpha-2}t \quad \text{as } t \to 0, \tag{51}$$

which confirms the formula (15a). Similarly, by combining (44), (49b) and (50), one obtains the late time approximation for variance for model (7)

$$\sigma_T^2(t) \sim \frac{V^2}{\beta^2}t^{2\gamma}\left[\frac{2}{\Gamma(2\gamma+1)} - \frac{1}{(\Gamma(\gamma+1))^2}\right] + \frac{D\alpha(\alpha-1)\lambda^{\alpha-2}}{\beta}\frac{t^{\gamma}}{\Gamma(\gamma+1)} \quad \text{as } t \to \infty, \tag{52}$$

which confirms the formula (15b).

Appendix C: Eulerian Approach to Solve the TFADE-Total Model (7)

We illustrate the Eulerian method using the TFADE-total model (7). First, discretize (7) using an implicit finite difference scheme

$$\frac{C_i^{n+1} - C_i^n}{\Delta t} + \frac{\beta}{(\Delta t)^{\gamma}}\sum_{k=0}^{n+1}[g_k C_i^{n-(k-1)}]$$
$$= -V\frac{C_i^{n+1} - C_{i-1}^{n+1}}{\Delta x} + D\left\{e^{-\lambda x_i}\frac{1}{h^{\alpha}}\sum_{j=0}^{i+1}[f_j e^{\lambda x_{i-(j-1)}}C_{i-(j-1)}^{n+1}]\right.$$
$$\left. - \lambda^{\alpha}C_i^{n+1} - \alpha\lambda^{\alpha-1}\frac{C_i^{n+1} - C_{i-1}^{n+1}}{\Delta x}\right\} + \frac{\beta(t_n)^{-\gamma}}{\Gamma(1-\gamma)}C_i^0, \tag{53}$$

where the one-shift Grünwald approximation [2] is used to approximate both the time (γ-order) and space (α-order) fractional derivatives. The Riemann-Liouville fractional derivative in time is used here, so that the shifted Grünwald approximation can be applied [2]. Here g_k and f_j are Grünwald weights. Also, Δt and Δx (note $\Delta x = h$) are time and space discretization sizes, respectively.

The above formula can be built for each node, resulting in a linear system of equations $\underline{A}\underline{C}^{n+1} = \underline{C}^n + \Delta t \underline{S}^{n+1}$ where

$$\underline{C}^L = [C_0^L, C_1^L, C_2^L, \ldots, C_K^L]^T; \quad L = n \text{ or } n+1 \text{ denotes the time step}$$

and $\underline{A} = [A_{i,j}]$ is the matrix of coefficients. These coefficients, for $i = 1, \ldots, K-1$ and $j = 1, \ldots, K-1$ are defined as follows:

$$A_{i,j} = \begin{cases} 0, & \text{when } j \geq i+2, \\ -\frac{\Delta t}{h^\alpha} D f_0 e^{\lambda h}, & \text{when } j = i+1, \\ 1 + \beta \frac{1}{(\Delta t)^{\gamma-1}} g_0 + V \frac{\Delta t}{h} - \Delta t D [\frac{1}{h^\alpha} f_1 - \lambda^\alpha - \alpha \lambda^{\alpha-1} \frac{1}{h}], & \text{when } j = i, \\ -V \frac{\Delta t}{h} - \Delta t D [\frac{1}{h^\alpha} f_2 e^{-\lambda h} + \alpha \lambda^{\alpha-1} \frac{1}{h}], & \text{when } j = i-1, \\ -\Delta t D \frac{1}{h^\alpha} f_{i-(j-1)} e^{-\lambda(i-j)h}, & \text{when } j \leq i-2 \end{cases}$$

while $A_{0,0} = 1$, $A_{0,j} = 0$ for $j = 1, \ldots, K$, $A_{K,K} = 1$, $A_{K,K-1} = -1$, and $A_{K,j} = 0$ for $j = 0, \ldots, K-2$.

Here we explore the stable criterion of the above scheme using the Greschgorin theorem [29]. The eigenvalues of the matrix $\underline{A}$ are in the disks centered at $A_{i,i}$ with radius $r_i = \sum_{k=0, k\neq i}^{K} A_{i,k}$. Firstly, we have

$$A_{i,i} - r_i = 1 + \beta \frac{1}{(\Delta t)^{\gamma-1}} + \Delta t D \lambda^\alpha - \Delta t D \frac{1}{h^\alpha} \sum_{j=0}^{i+1} [f_{i-j+1} e^{-\lambda(i-j)h}]. \tag{54}$$

To meet the criterion of $A_{i,i} - r_i > 1$, the following formula must be true:

$$\beta \frac{1}{(\Delta t)^{\gamma-1}} + \Delta t D \lambda^\alpha - \Delta t D \frac{1}{h^\alpha} \sum_{j=0}^{i+1} [f_{i-j+1} e^{-\lambda(i-j)h}] > 0, \tag{55}$$

which requires

$$\Delta t < \beta^{1/\gamma} \left[\frac{1}{h^\alpha} D e^{\lambda h} - D \lambda^\alpha \right]^{-1/\gamma}. \tag{56}$$

Secondly, we have

$$\begin{aligned} A_{i,i} + r_i = 1 + \beta \frac{1}{(\Delta t)^{\gamma-1}} + 2V \frac{\Delta t}{h} + 2\Delta t D \alpha \lambda^{\alpha-1} \frac{1}{h} + \Delta t D \lambda^\alpha - \Delta t D \frac{1}{h^\alpha} f_1 \\ + \frac{\Delta t}{h^\alpha} D f_0 e^{\lambda h} + \frac{\Delta t}{h^\alpha} D f_2 e^{-\lambda h} + \Delta t D \frac{1}{h^\alpha} \sum_{j=0}^{i-2} [f_{i-j+1} e^{-\lambda(i-j)h}]. \end{aligned} \tag{57}$$

Since the Grünwald weights $f_0 = 1$, $f_1 = -\alpha$ (so $-2 < f_1 < -1$), $f_2 = \alpha(\alpha-1)/2 > 0$, and $f_i > 0$ for $i > 2$, we have all the terms on the RHS of (57) larger than zero. Therefore,

$$A_{i,i} + r_i > 1. \tag{58}$$

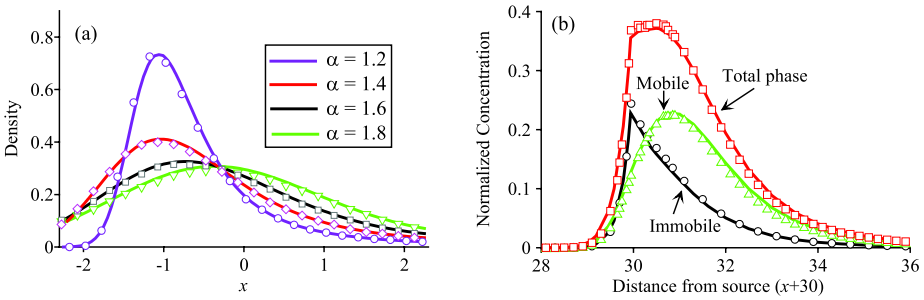

Fig. 9 Eulerian solutions (*lines*) versus Lagrangian solutions (*symbols*). (**a**) The density of the tempered α-stable, with the truncation parameter $\lambda = 0.0001$ and various scale indexes α. (**b**) Snapshots of particle plumes governed by the TFADE-Total model (7) (Total phase) and the TFADE-Mobile model (8) (mobile phase). Parameters are: $\gamma = 0.5$, $\beta = 0.5$, $\alpha = 1.3$, $V = 2$, $D = 2$, $\lambda = 0.1$, and $t = 1$. The immobile phase concentration is the difference between the total and mobile concentrations

Hence the magnitude of eigenvalues of $\underline{A}$ are no less than 1 if the time step Δt is small enough to meet the criterion of (56). The spectral radius of the inverse matrix $\underline{A}^{-1}$ is no larger than 1 and any error in w^{n+1} is not magnified. Hence the above Eulerian numerical scheme is conditionally stable.

The TFADE-Mobile model (8) can be solved following the above scheme. By deleting the last term on the RHS of (53), the resultant finite difference scheme is also conditionally stable with the same stability criterion.

The above Eulerian scheme has been used extensively to cross verify the Lagrangian solutions developed in Sect. 4. A few examples are shown in Fig. 9. Figure 9a shows the tempered stable density, which is equal to the solution of the simplified TFADE (37) with $V = 0$, $D = 1$, and $t = 1$. Figure 9b shows the simulated particle snapshots at all phases, where the particle plume in the mobile phase moves relatively faster than the plume in the immobile phase. A general match for solutions can be found for the two different numerical solvers.

References

1. Adams, E.E., Gelhar, L.W.: Field study of dispersion in a heterogeneous aquifer: 2. Spatial moment analysis. Water Resour. Res. **28**(12), 3293–3307 (1992)
2. Baeumer, B., Meerschaert, M.M.: Tempered stable Lévy motion and transient super-diffusion. J. Comput. Appl. Math. **233**, 2438–2448 (2010)
3. Boggs, J.M., Adams, E.E.: Field study of dispersion in a heterogeneous aquifer: 4. Investigation of adsorption and sampling bias. Water Resour. Res. **28**(12), 3325–3336 (1992)
4. Boggs, J.M., Young, S.C., Beard, L.M.: Field study of dispersion in a heterogeneous aquifer: 1. Overview and site description. Water Resour. Res. **28**(12), 3281–3291 (1992)
5. Boyarchenko, S., Levendorskiĭ, S.: Non-Gaussian Merton-Black-Scholes Theory. World Scientific, River Edge (2002), Chap. 3, pp. 421
6. Boyarchenko, S., Levendorskiĭ, S.: Barrier options and touch-and-out options under regular Lévy processes of exponential type. Ann. Appl. Probab. **12**(4), 1261–1298 (2002)
7. Bruno, R., Sorriso-Valvo, L., Carbone, V., Bavassano, B.: A possible truncated-Levy-flight statistics recovered from interplanetary solar-wind velocity and magnetic-field fluctuations. Europhys. Lett. **66**(1), 146–152 (2004)
8. Carr, P., Wu, L.: The finite moment log stable process and option pricing. J. Finance **58**(2), 753–778 (2003)
9. Cartea, A., del-Castillo-Negrete, D.: Fractional diffusion models of option prices in markets in markets with jumps. Physica A **374**, 749–763 (2007)

10. Cartea, A., del-Castillo-Negrete, D.: Fluid limit of the continuous-time random walk with general Lévy jump distribution functions. Phys. Rev. E **76**, 041105 (2007)
11. Chang, F.X., Chen, J., Huang, W.: Anomalous diffusion and fractional advection-diffusion equation. Acta Phys. Sin. **54**(3), 1113–1117 (2005)
12. Chechkin, A.V., Klafter, J., Gonchar, V.Y., Metzler, R., Tanatarov, L.V.: Bifurcation, bimodality and finite variance in confined Lévy flights. Phys. Rev. E **67**, 010102 (2003)
13. Chechkin, A.V., Gonchar, V.Y., Klafter, J., Metzler, R., Tanatarov, L.V.: Lévy flights in a steep potential well. J. Stat. Phys. **115**(516), 1505–1535 (2004)
14. Chechkin, A.V., Gonchar, V.Y., Klafter, J., Metzler, R.: Natural cutoff in Lévy flights caused by dissipative nonlinearity. Phys. Rev. E **72**, 010101 (2005)
15. Chechkin, A.V., Gonchar, V.Y., Gorenflo, R., Korabel, L., Sokolov, I.M.: Generalized fractional diffusion equations for accelerating subdiffusion and truncated Lévy flight. Phys. Rev. E **78**, 021111 (2008)
16. Cushman, J.H., Moroni, M.: Statistical mechanics with three-dimensional particle tracking velocimetry experiments in the study of anomalous dispersion. I. Theory. Phys. Fluid **13**(1), 75–80 (2001)
17. Cushman, J.H., Hu, B.X., Ginn, T.R.: Nonequilibrium statistical mechanics of preasymptotic dispersion. J. Stat. Phys. **75**(5/6), 859–878 (1994)
18. Del-Castillo-Negrete, D.: Truncation effects in superdiffusive front propagation with Lévy flights. Phys. Rev. E **79**(3), 031120 (2009)
19. Deng, Z.Q., Lima, J., Lima, M., Singh, V.P.: A fractional dispersion model for overland solute transport. Water Resour. Res. **42**, W03416 (2006). doi:10.1029/2005WR004146
20. Feller, W.: An Introduction to Probability Theory and Its Applications, vol. II, 2nd edn. Wiley, New York (1971), Chap. VII
21. Garabedian, S.P., LeBlanc, D.R., Gelhar, L.W., Celia, M.A.: Large-scale natural gradient tracer test in sand and gravel. Cape Cod, Massachusetts, 2. Analysis of spatial moments for a nonreactive tracer. Water Resour. Res. **27**(5), 911–924 (1991)
22. Gorenflo, R., Mainardi, F.: Fractional calculus, integral and differential equations of fractional order. In: Carpinteri, A., Mainardi, F. (eds.) Fractals and Fractional Calculus in Continuum Mechanics, pp. 223–276. Springer, Wien (1997)
23. Gorenflo, R., Vivoli, A., Mainardi, F.: Discrete and continuous random walk models for space-time fractional diffusion. Nonlinear Dyn. **38**, 101–116 (2004)
24. Haggerty, R., McKenna, S.A., Meigs, L.C.: On the late-time behavior of tracer test breakthrough curves. Water Resour. Res. **36**, 3467–3479 (2000)
25. Harvey, C.F., Gorelick, S.M.: Rate-limited mass transfer or macrodispersion: which dominates plume evolution at the Macrodispersion Experiment (MADE) site? Water Resour. Res. **36**(3), 637–650 (2000)
26. Herrick, M.G., Benson, D.A., Meerschaert, M.M., McCall, K.R.: Hydraulic conductivity, velocity, and the order of the fractional dispersion derivative in a highly heterogeneous system. Water Resour. Res. **38**(11), W1227 (2002). doi:10.1029/2001WR000914
27. Huang, G.H., Huang, Q.Z., Zhan, H.B.: Evidence of one-dimensional scale-dependent fractional advection-dispersion. J. Contam. Hydrol. **85**, 53–71 (2006)
28. Inoue, J., Sazuka, N.: Crossover between Lévy and Gaussian regimes in first-passage processes. Phys. Rev. E **76**, 021111 (2007)
29. Isaacson, E., Keller, H.B.: Analysis of Numerical Methods. Wiley, New York (1966), pp. 153–156
30. Kleinhans, D., Friedrich, R.: Continuous-time random walks: Simulation of continuous trajectories. Phys. Rev. E **76**, 06112 (2007)
31. Kim, S., Kavvas, M.L.: Generalized Fick's law and fractional ADE for pollutant transport in a river: detailed derivation. J. Hydrol. Eng. **11**(1), 80–83 (2006)
32. Kohlbecker, M., Wheatcraft, S.W., Meerschaert, M.M.: Heavy tailed log hydraulic conductivity distributions imply heavy tailed log velocity distributions. Water Resour. Res. **42**, W04411 (2006). doi:10.1029/2004WR003815
33. Koponen, I.: Analytic approach to the problem of convergence of truncated Lévy flights towards the Gaussian stochastic process. Phys. Rev. E **52**(1), 1197–1198 (1995)
34. Krepysheva, N., Di Pietro, L., Néel, M.C.: Space-fractional advection-diffusion and reflective boundary condition. Phys. Rev. E **73**, 021104 (2006)
35. LeBlanc, D.R., Garabedian, S.P., Hess, K.M., Gelhar, L.W., Qaudri, R.D., Stollenwerk, K.G., Wood, W.W.: Large-scale natural gradient tracer test in sand and gravel. Cape Cod, Massachusetts, 1. Experimental design and observed tracer movement. Water Resour. Res. **27**(5), 895–910 (1991)
36. Magdziarz, M., Weron, A.: Competition between subdiffusion and Lévy flights: A Monte Carlo approach. Phys. Rev. E **75**, 056702 (2007)
37. Mandelbrot, B.: Fractals and Scaling in Finance, 1st edn. Springer, Berlin (1997)
38. Mantegna, R.N., Stanley, H.E.: Stochastic process with ultraslow convergence to a Gaussian: The truncated Lévy flight. Phys. Rev. Lett. **73**(22), 2946–2949 (1994)

39. Mantegna, R.N., Stanley, H.E.: Scaling behavior in the dynamics of an economic index. Nature **376**(6535), 46–49 (1995)
40. Mariani, M.C., Liu, Y.: Normalized truncated Levy walks applied to the study of financial indices. Physica A **377**, 590–598 (2007)
41. Marom, O., Momoniat, E.: A comparison of numerical solutions of fractional diffusion models in finance. Nonlinear Anal.-Real. **10**, 3435–3442 (2009)
42. Matsushita, R., Rathie, P., Da Silva, S.: Exponentially damped Lévy flights. Physica A **326**, 544–555 (2003)
43. Matsushita, R., Gleria, I., Figueiredo, A., Rathie, P., Da Silva, S.: Exponentially damped Lévy flights, multiscaling, and exchange rates. Physica A **333**, 353–369 (2004)
44. Metzler, R., Klafter, J.: The random walk's guide to anomalous diffusion: A fractional dynamic approach. Phys. Rep. **339**, 1–77 (2000)
45. Metzler, R., Klafter, J.: The restaurant at the end of the random walk: Recent development in fractional dynamics of anomalous transport processes. J. Phys. A **37**, R161–R208 (2004)
46. Metzler, R., Chechkin, A.V., Klafter, J.: Slow and fast: Foundation and properties of subdiffusion and Lévy flights. In: Encyclopaedia on Complexity, pp. 1–35 (2007). arXiv:0706.3553v1
47. Miller, K.S., Ross, B.: An Introduction to Fractional Calculus and Fractional Differential Equations. Wiley, Hoboken (1993)
48. Moroni, M., Cushman, J.H.: Three-dimensional particle tracking velocimetry studies of the transition from pore dispersion to Fickian dispersion for homogeneous porous media. Water Resour. Res. **37**(4), 873–884 (2001)
49. Pachepsky, Y., Timlin, D., Benson, D.A.: Transport of water and solutes in soils as in fractal porous media. Soil Sci. Soc. Am. J. **56**, 51–75 (2001)
50. Podlubny, I.: Fractional Differential Equations. Academic Press, San Diego (1999), p. 366
51. Rehfeldt, K.R., Boggs, J.M., Gelhar, L.W.: Field study of dispersion in a heterogeneous aquifer: 3. Geostatistical analysis of hydraulic conductivity. Water Resour. Res. **28**(12), 3309–3324 (1992)
52. Rosiński, J.: Tempering stable processes. Stoch. Proc. Appl. **117**, 677–707 (2007)
53. Scalas, E., Gorenflo, R., Mainardi, F.: Uncoupled continuous-time random walks: Solution and limiting behavior of the master equation. Phys. Rev. E **69**, 011107 (2004)
54. Schoutens, W.: Lévy Processes in Finance: Pricing Financial Derivatives. Wiley, Chichester (2003). Chap. 5, p. 170
55. Schumer, R., Benson, D.A., Meerschaert, M.M., Baeumer, B.: Eulerian derivation of the fractional advection-dispersion equation. J. Contam. Hydrol. **48**, 69–88 (2001)
56. Schumer, R., Benson, D.A., Meerschaert, M.M., Baeumer, B.: Fractal mobile/immobile solute transport. Water Resour. Res. **39**(10), 1296 (2003). doi:10.1029/2003WR002141
57. Sokolov, I.M., Chechkin, A.V., Klafter, J.: Fractional diffusion equation for a power-law-truncated Lévy processes. Physica A **336**(3–4), 245–251 (2004)
58. Zhan, H.B.: On the ergodicity hypothesis in heterogeneous formations. Math. Geol. **31**(1), 113–134 (1999)
59. Zhang, X.X., Crawford, J.W., Deeks, L.K., Sutter, M.I., Bengough, A.G., Young, I.M.: A mass balance based numerical method for the fractional advection-dispersion equation: theory and application. Water Resour. Res. **41**, W07029 (2005). doi:10.1029/2004WR003818
60. Zhang, Y., Benson, D.A., Meerschaert, M.M., Scheffler, H.P.: On using random walks to solve the space-fractional advection-dispersion equations. J. Stat. Phys. **123**(1), 89–110 (2006). doi:10.1007/s10955-006-9042-x
61. Zhang, Y., Meerschaert, M.M., Baeumer, B.: Particle tracking for time-fractional diffusion. Phys. Rev. E **78**, 036705 (2008)
62. Zhang, Y., Benson, D.A., Reeves, D.M.: Time and space nonlocalities underlying fractional derivative models: Distinction and literature review of field applications. Adv. Water Resour. **32**, 561–581 (2009)
63. Zhou, L., Selim, H.M.: Application of the fractional advection-dispersion equation in porous media. Soil Sci. Soc. Am. J. **67**, 1079–1084 (2003)